Check for updates

Modification of the Expression of the Aquaporin ZmPIP2;5 Affects Water Relations and Plant Growth[1[OPEN]]

Lei Ding,[a,2] Thomas Milhiet,[a,2] Valentin Couvreur,[b] Hilde Nelissen,[c,d] Adel Meziane,[a,e] Boris Parent,[e] Stijn Aesaert,[c,d] Mieke Van Lijsebettens,[c,d] Dirk Inzé,[c,d] François Tardieu,[e] Xavier Draye,[b] and François Chaumont[a,3,4]

[a]Louvain Institute of Biomolecular Science and Technology, Université catholique de Louvain, 1348 Louvain-la-Neuve, Belgium
[b]Earth and Life Institute, Université catholique de Louvain, 1348 Louvain-la-Neuve, Belgium
[c]Center for Plant Systems Biology, Vlaams Instituut voor Biotechnologie-Ghent University, 9052 Ghent, Belgium
[d]Department of Plant Biotechnology and Bioinformatics, Ghent University, 9052 Ghent, Belgium
[e]Laboratoire d'Ecophysiologie des Plantes sous Stress Environnementaux (LEPSE), Université de Montpellier, Institut National de la Recherche Agronomique (INRA), F-34000 Montpellier, France

ORCID IDs: 0000-0003-1262-5289 (L.D.); 0000-0002-1087-3978 (V.C.); 0000-0001-7494-1290 (H.N.); 0000-0002-7600-9592 (B.P.); 0000-0001-8787-7347 (S.A.); 0000-0002-7632-1463 (M.V.L.); 0000-0002-3217-8407 (D.I.); 0000-0002-7287-0094 (F.T.); 0000-0002-3637-3330 (X.D.); 0000-0003-0155-7778 (F.C.).

The plasma membrane intrinsic protein PIP2;5 is the most highly expressed aquaporin in maize (*Zea mays*) roots. Here, we investigated how deregulation of PIP2;5 expression affects water relations and growth using maize overexpression (OE; B104 inbred) or knockout (KO; W22 inbred) lines. The hydraulic conductivity of the cortex cells of roots grown hydroponically was higher in PIP2;5 OE and lower in *pip2;5* KO lines compared with the corresponding wild-type plants. While whole-root conductivity decreased in the KO lines compared to the wild type, no difference was observed in OE plants. This paradox was interpreted using the MECHA hydraulic model, which computes the radial flow of water within root sections. The model hints that the plasma membrane permeability of the cells is not radially uniform but that PIP2;5 may be saturated in cell layers with apoplastic barriers, i.e. the endodermis and exodermis, suggesting the presence of posttranslational mechanisms controlling the abundance of PIP in the plasma membrane in these cells. At the leaf level, where the *PIP2;5* gene is weakly expressed in wild-type plants, the hydraulic conductance was higher in the PIP2;5 OE lines compared with the wild-type plants, whereas no difference was observed in the *pip2;5* KO lines. The temporal trend of leaf elongation rate, used as a proxy for that of xylem water potential, was faster in PIP2;5 OE plants upon mild stress, but not in well-watered conditions, demonstrating that PIP2;5 may play a beneficial role in plant growth under specific conditions.

Aquaporins, which belong to the plasma membrane intrinsic protein (PIP) subfamily, are major actors controlling membrane water permeability. The physiological functions of PIPs are straightforward at the cell level (Hachez et al., 2006a, 2008, 2012; Heinen et al., 2014), but are considerably more complex at the organ and whole-plant levels. For example, overexpression (OE) or silencing of PIP aquaporins has contrasting effects on root hydraulics (Siefritz et al., 2002; Hachez et al., 2006b; Postaire et al., 2010; Sade et al., 2010), root development (Péret et al., 2012), leaf hydraulic conductance (K_{leaf}; Prado and Maurel, 2013; Sade et al., 2014), stomatal movement (Grondin et al., 2015; Wang et al., 2016; Rodrigues et al., 2017), and transpiration (T_r; Maurel et al., 2016). This is largely because the transcellular path, in which water crosses the cell membranes mainly through aquaporins (Steudle and Peterson, 1998; Steudle, 2000), occurs simultaneously with the other two pathways, namely the apoplastic path, in which water flow goes through the cell wall, and the symplastic path, in which water moves through the plasmodesmata. The overall root hydraulic conductivity (L_{pr}) is the integration of conductivity from the three pathways; their contribution to the L_{pr} varies according to root anatomy development and environmental factors (drought, high salinity, nutrient availability, anoxia, etc.). To better understand the complexity of root radial hydraulic conductivity and integrate the multiple variables, mathematical models have been developed (Steudle and Peterson, 1998; Zwieniecki et al., 2002; Foster and Miklavcic, 2017; Couvreur et al., 2018). Among these models, the MECHA model (Couvreur et al., 2018) predicts the root radial hydraulic conductivity based on the detailed radial anatomy of the root and the distribution of the cell wall hydraulic conductivity, the cell plasma membrane permeability, the hydraulic conductance, the frequency of plasmodesmata, and the membrane reflection coefficients. MECHA is therefore appropriate for addressing subcellular hydraulics and its impact on the radial transport of water.

Here, we analyzed the effects of OE or silencing of maize (*Zea mays*) PIP2;5 at both the cellular and

 © 2020 American Society of Plant Biologists. All Rights Reserved.

Downloaded from https://academic.oup.com/plphys/article/182/4/2154/6116623 by universite catholique de louvain user on 08 October 2021

whole-plant levels. The *PIP2;5* gene encodes an active water channel (Fetter et al., 2004), is the most expressed *PIP* gene in the primary root (Hachez et al., 2006a), and shows a polarized localization at the plasma membrane side facing the external medium, supporting its function in root water uptake. Another clue that PIP2;5 is involved in radial water movement is its high expression in cell types with Casparian strips (exodermis and endodermis), places where water has to enter the symplast to continue its flow to the xylem vessels (Hachez et al., 2012). In roots, the expression of *PIP2;5* mRNA and its protein abundance are modulated by diurnal and circadian rhythms, osmotic stress, and growth conditions (aeroponic and hydroponic; Hachez et al., 2012; Caldeira et al., 2014b). In addition, PIP2;5 proteins are more abundant in maize lines overexpressing the abscisic acid biosynthesis gene and less abundant in those silenced for it (Parent et al., 2009). The *PIP2;5* gene is weakly expressed in leaves, with a maximum of expression at the end of the elongation zone and the zone where the leaf emerges from the sheath and where lignification of the metaxylem is observed (Hachez et al., 2008). Altogether, these data suggest that PIP2;5 plays important roles in regulating water relations in maize, but genetic approaches to further understand its physiological function are missing.

We first characterized PIP2;5 OE and *pip2;5* knockout (KO) lines at the molecular and cellular levels and addressed the question of the effects of the manipulation of PIP2;5 expression at the plant level by collectively examining the hydraulic conductance in roots and leaves and the time course of leaf elongation rate (LER), considered here as a way to indirectly assess the changes in xylem water potential following fluctuations of the evaporative demand (Caldeira et al., 2014a, 2014b). While the cell hydraulic conductivity was affected by deregulation of PIP2;5 expression, the contrasting results at the organ level suggest that upscaling requires a modeling approach to decipher the dataset presented here.

RESULTS

Generation, Isolation, and Molecular Characterization of Maize Lines Deregulated in PIP2;5 Expression

To determine the role of PIP2;5 aquaporin in maize, we first prepared a genetic construct aimed at constitutive OE of the *PIP2;5* gene under the control of the *p35S* promoter (Fig. 1A) and performed an *Agrobacterium*-mediated transformation of the inbred B104. Two independent *PIP2;5* OE lines (OE-4 and OE-13) with high PIP2;5 protein content based on western blotting analysis (see below in this section) were selected for further molecular characterization. In addition, we obtained from the Maize Genetics Cooperation Stock Center (http://maizecoop.cropsci.uiuc.edu/) a putative *pip2;5* KO W22 inbred line (UFMu00767) containing a *Mu* transposon in the *PIP2;5* gene (Fig. 1B). The presence and the site of insertion of the *Mu* transposon in the *PIP2;5* gene was determined by PCR amplification of genomic DNA using *PIP2;5* and *Mu* specific primers; this showed that the *Mu* transposon was inserted in the second intron of the *PIP2;5* gene (Fig. 1B).

To confirm OE and down-regulation of *PIP2;5* in the maize lines, microsomal fractions were prepared from roots and leaves, and PIP2;5 was immunodetected using specific antibodies (Hachez et al., 2006a). In roots, where endogenous *PIP2;5* is the highest-expressed *PIP* gene, increases in PIP2;5 protein abundance of 17% and 141% were observed in the PIP2;5 OE-4 and OE-13 lines, respectively, compared with the nontransgenic segregating siblings (wild-type B104; Fig. 1C). In leaves, where the endogenous *PIP2;5* is lowest expressed, >10-fold higher PIP2;5 protein abundance was detected in the PIP2;5 OE-4 and OE-13 lines compared with the wild-type B104 plants (Fig. 1D). On the other hand, the PIP2;5 protein level was 9-fold lower in roots of the *pip2;5* KO line than in roots of nontransgenic segregating siblings (wild-type W22; Fig. 1C). No significant difference in PIP2;5 signal intensity was found between *pip2;5* KO and wild-type W22 leaves (Fig. 1D), but the PIP2;5 signals in leaves were hardly detectable and only observed after a very long exposure.

We also analyzed the *PIP2;5* mRNA levels in roots and leaves by reverse-transcription quantitative PCR (RT-qPCR). In the OE plants, while no difference in *PIP2;5* endogenous mRNA levels were observed, a high *PIP2;5* transgene mRNA signal was detected using a *PIP2;5*-specific forward primer and a construct linker-specific reverse primer (Supplemental Fig. S1, A–D). No amplification was detected with this pair of primers in the wild-type B104 plants. In *pip2;5* KO plants, we

[1]This work was supported by the Belgian National Fund for Scientific Research(FNRS; FRFC 2.4.501.06F and FC 84104 to V.C.), the Interuniversity Attraction Poles Programme-Belgian Science Policy (grant IAP7/29), the "Communauté française de Belgique-Actions de Recherches Concertées" (grants ARC11/16-036 and ARC16/21-075), the Pierre and Colette Bauchau Award, an Incoming Post-doc Move-in Louvain Fellowship co-funded by the Marie Curie Actions (to L.D.), and a research fellowship at the Fonds de Formation à la Recherche dans l'Industrie et l'Agriculture (to T.M.).

[2]These authors contributed equally to the article.

[3]Author for contact: francois.chaumont@uclouvain.be.

[4]Senior author.

The author responsible for distribution of materials integral to the findings presented in this article in accordance with the policy described in the Instructions for Authors (www.plantphysiol.org) is: François Chaumont (francois.chaumont@uclouvain.be).

L.D., T.M., H.N., B.P., and F.C. designed the experiments; L.D., T.M., H.N., A.M., B.P., and S.A. performed the experiments; M.V.L. supervised the maize transformation; L.D., T.M., V.C., H.N., A.M., B.P., S.A., F.T., X.D., M.V.L., and F.C. analyzed the data; L.D. and F.C. wrote the article; and all authors contributed to the discussion and revision of the manuscript.

[OPEN]Articles can be viewed without a subscription.

www.plantphysiol.org/cgi/doi/10.1104/pp.19.01183

Downloaded from https://academic.oup.com/plphys/article/182/4/2154/6116623 by universite catholique de louvain user on 08 October 2021

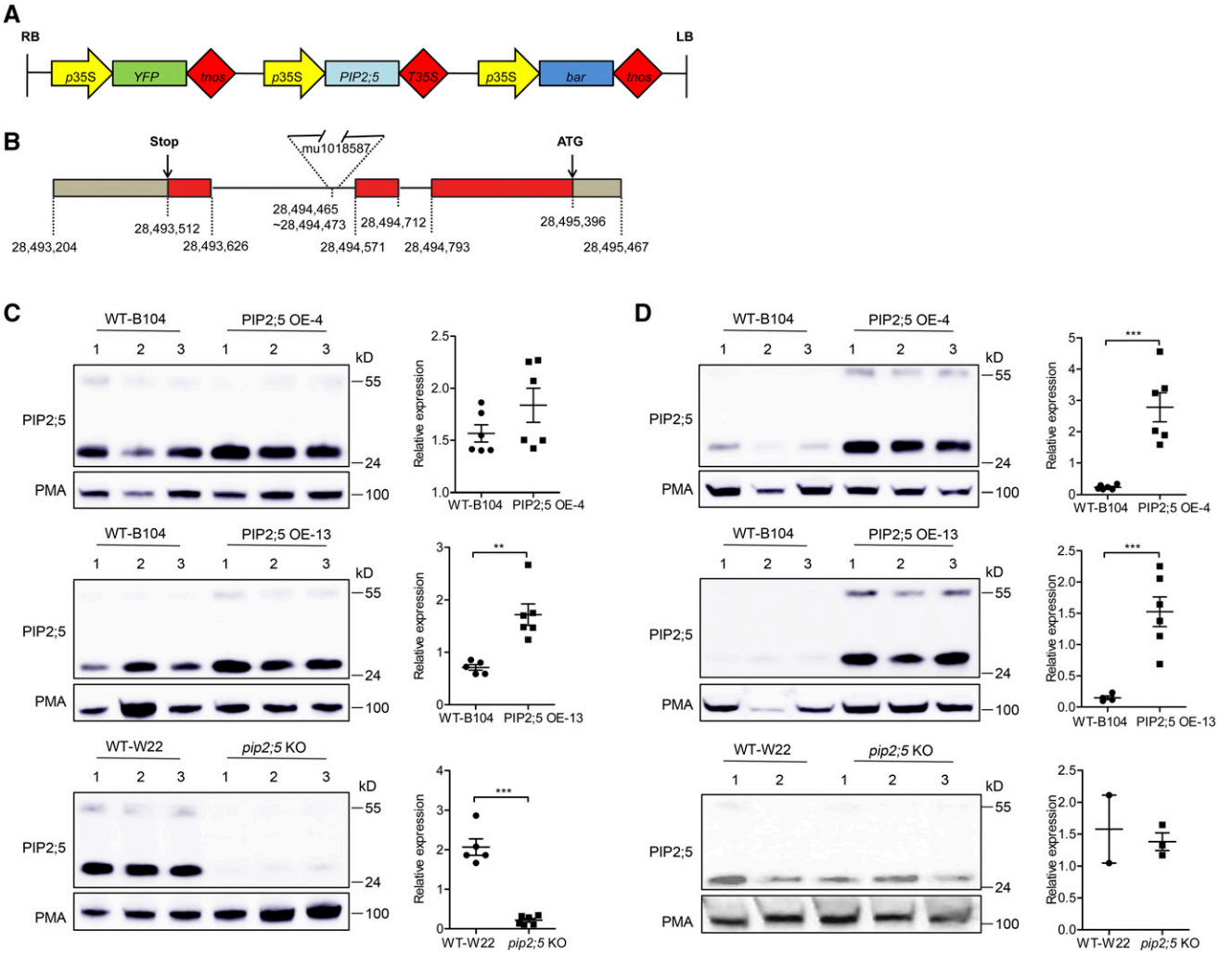


Figure 1. PIP2;5 protein levels in the maize lines deregulated in its expression. A, Schematic representation of the transfer DNA used to overexpress PIP2;5 in the B104 maize line. YFP, Yellow fluorescent proteins; *tnos*, terminator of the nopaline gene; *bar*, gene conferring resistance to bialaphos. B, Genomic structure of the *PIP2;5* gene with the position of the Mu transposon insertion in the *pip2;5* KO line (W22 background). The data source of gene position and insertion site is from "Maize B73 RefGen_v3" in MaizeGDB (https://maizegdb.org/). The *PIP2;5* exons are in red. C and D, PIP2;5 protein level in root (C) and leaf (D) in the wild type (WT; indicated by wild-type B104 and wild-type W22), two PIP2;5 OE lines (OE-4 and OE-13), and a *pip2;5* knockout line (*pip2;5* KO). The plants were cultured under hydroponic conditions and the microsomal fractions were extracted from primary roots and leaves of 1-week-old seedlings. Proteins (20 μg [C] or 30 μg [D]) were subjected to western blotting using antibodies raised against PIP2;5 or PMA (H^+-ATPases). The PMA signal was used to control the gel loading and normalize the PIP2;5 signals (plots at right). In the quantification panels, data are expressed as the mean $\pm$ SE of two independent experiments, each experiment containing two to three plants for each maize line. Significant differences among the treatments are indicated by $^{**}P < 0.01$ and $^{***}P < 0.001$.

observed 2,175-fold and 5-fold lower mRNA level in roots (Supplemental Fig. S1E) and leaves (Supplemental Fig. S1F), respectively, compared to the wild-type W22 plants. To investigate the reason why a very faint protein signal was still observed in the leaf extract by immunodetection, we performed RT-qPCR with primers flanking the Mu insertion site and detected a weak signal (Supplemental Fig. S2), suggesting that the *pip2;5* KO plants are not a complete loss-of-function line.

To investigate whether the expression of other PIPs was affected by the deregulation of *PIP2;5* gene in both roots and leaves, RT-qPCR and western blotting were performed. No significant difference in the mRNA levels of most *PIPs* was observed between PIP2;5 OE lines or *pip2;5* KO and their corresponding wild-type lines in both roots and leaves (Supplemental Fig. S1). Similarly, at the protein level, no significant difference in PIP1;2 and PIP2;1/2;2 was observed between the OE or KO lines and their respective wild-type plants (Supplemental Fig. S3).

Because we used two different maize genetic backgrounds in this work, we checked that the expression

Downloaded from https://academic.oup.com/plphys/article/182/4/2154/6116623 by universite catholique de louvain user on 08 October 2021

pattern of PIP2;5 was similar in the W22 and B73 lines (Hachez et al., 2006a, 2008, 2012). Similar to the previous results obtained in the B73 line, an intense signal of PIP2;5 was immunodetected in the exo- and endodermis cells of W22 root, where the lignin and suberin are deposited (Supplemental Fig. S4, A and B). *PIP2;5* was also the most highly expressed *PIP* gene in W22 roots and was weakly expressed in leaves (Supplemental Fig. S4C).

Altered Hydraulic Conductance in the PIP2;5 Deregulated Plants

We first investigated the effect of PIP2;5 deregulation on the hydraulic conductivity of the root cortex cell (L_{pc}), measured with a cell pressure probe. The half-time of water exchange ($T_{1/2}$) across the membrane of root cortex cells was 1.9 to 1.8 times shorter (faster water flow) in the two PIP2;5 OE lines than in wild-type B104, whereas $T_{1/2}$ was 2.8 times longer (slower water flow) in the *pip2;5* KO line with respect to wild-type W22 (Table 1). As a result, the L_{pc} was 69% and 67% higher in PIP2;5 OE-4 and OE-13 lines, respectively (Fig. 2, A and B). In contrast, the L_{pc} decreased by 63% in the *pip2;5* KO line compared with the wild-type W22 (Fig. 2C). The turgor pressure and the cell elastic modulus (ε) were not affected by the deregulation of PIP2;5 expression (Table 1), except that the $\varepsilon_{corrected}$ was higher in PIP2;5 OE-13 lines than in wild-type B104 plants. In addition, a bigger cell volume was measured in PIP2;5 OE-13 lines compared to wild-type B104 plants, suggesting that PIP2;5 OE in this line has affected root cell expansion. Consistently, the membrane water permeability of leaf mesophyll protoplasts (P_{os}) was significantly higher in both PIP2;5 OE lines (85% for OE-4 and 60% for OE-13) than in wild-type B104 plants (Fig. 2, D and E). On the other hand, no difference in P_{os} was observed between the wild-type W22 and *pip2;5* KO lines (Fig. 2F) due to the fact that *PIP2;5* is barely expressed in wild-type leaves. It is worth mentioning that the L_{pc} and P_{os} mean values were higher in wild-type W22 than in wild-type B104, suggesting that the two inbred lines have different intrinsic membrane permeabilities.

Consistent with the results at the cell level, the leaf hydraulic conductance (K_{leaf}), measured with a hydraulic conductance flowmeter (HCFM), increased by 58% and 171% in the PIP2;5 OE-4 and OE-13 lines, respectively, compared with the K_{leaf} of wild-type B104 plants (Fig. 3, D and E), whereas no significant difference in K_{leaf} was found between *pip2;5* KO plants and wild-type W22 plants (Fig. 3F). However, at the root level, the increase in L_{pc} did not result in a significant difference in the whole root conductance (L_{pr}) between wild-type B104 and the PIP2;5 OE lines (Fig. 3, A and B). Conversely, L_{pr} was significantly lower in the *pip2;5* KO line than in wild-type W22 (Fig. 3C).

The lack of correlation between cortex L_{pc} and L_{pr} in PIP2;5 OE plants is not straightforwardly deciphered. There are two reasons for this: (1) There are multiple hydraulic media in series across the root radius (including cell walls, membranes, and plasmodesmata), whose hydraulic conductivity may vary in each cell layer. L_{pr} is mostly sensitive to the hydraulic conductivity of media that limit water flow the most (e.g. at gatekeeper cell layers, i.e. endodermis and exodermis, where water flow through cell walls is limited by apoplastic barriers). (2) Root hydraulic media are arranged both in series and in parallel, so that water pathways may bypass some of the most limiting media (e.g. at gatekeeper cells, water may bypass cell walls by flowing through membranes, and a fraction of water flow also bypasses gatekeeper cell membranes by using a symplastic path). Hence, the quantitative modeling tool MECHA (Couvreur et al., 2018) with subcellular resolution of water flow was needed to statistically validate the significance of hypotheses offered to explain the lack of correlation between cortex L_{pc} and L_{pr} in wild-type and PIP2;5 OE plants. Hypothesis A considered that plasma membrane L_{pc} is uniform across cell layers (Fig. 4A), while hypothesis B considered that PIP2;5 is already "saturated" in wild-type gatekeeper cells (their L_{pc} equals that measured in the cortex of PIP2;5 OE lines) and "unsaturated" in other cell layers (their L_{pc} equals that measured in the wild-type cortex; Fig. 4E). Three values of cell wall hydraulic conductivity (k_{w1}–k_{w3}), spanning a range from the literature, were considered for each hypothesis. Statistical analysis of results from this combined modeling and experimental approach suggested that, given the observed L_{pc} in wild-type B104 and PIP2;5 OE plants, radially uniform patterns of cell membrane permeability may not account for the observed contrast between L_{pr} in wild-type B104 and that in the PIP2;5 OE-4 line,

Table 1. *Cell pressure probe measurements of maize root cortex cells in the wild type, PIP2;5 OE lines, and* pip2;5 *KO*

Root cortical cells from the third to sixth cell layer were punctured in the morning. The values are means ± SE (n = 10–15 cells from three to five plants). Significant difference ($P < 0.05$) among the treatments is indicated by lowercase letters. WT, wild type.

Line	Turgor Pressure (MPa)	$T_{1/2}$ (s)	Cell Volume (10^{-14} m^3)	Cell Surface Area (10^{-8} m^2)	$\varepsilon_{measured}$ (MPa)	$\varepsilon_{corrected}$ (MPa)
WT-B104	0.37 ± 0.01a	1.70 ± 0.14a	8.38 ± 1.63a	1.40 ± 0.17a	1.24 ± 0.20a	1.80 ± 0.30a
PIP2;5 OE-4	0.35 ± 0.01a	0.89 ± 0.07b	6.16 ± 1.07a	1.17 ± 0.12a	0.89 ± 0.06a	1.74 ± 0.09a
WT-B104	0.40 ± 0.01a	1.75 ± 0.15a	6.46 ± 0.81b	1.11 ± 0.09b	0.98 ± 0.12a	1.43 ± 0.16b
PIP2;5 OE-13	0.42 ± 0.01a	0.97 ± 0.08b	9.47 ± 0.94a	1.41 ± 0.10a	1.49 ± 0.23a	2.74 ± 0.35a
WT-W22	0.37 ± 0.01a	0.90 ± 0.08b	9.60 ± 0.88a	1.35 ± 0.09a	1.38 ± 0.18a	2.74 ± 0.38a
pip2;5 KO	0.34 ± 0.02a	2.56 ± 0.11a	8.29 ± 0.46a	1.21 ± 0.05a	1.61 ± 0.12a	2.14 ± 0.19a

Downloaded from https://academic.oup.com/plphys/article/182/4/2154/6116623 by universite catholique de louvain user on 08 October 2021

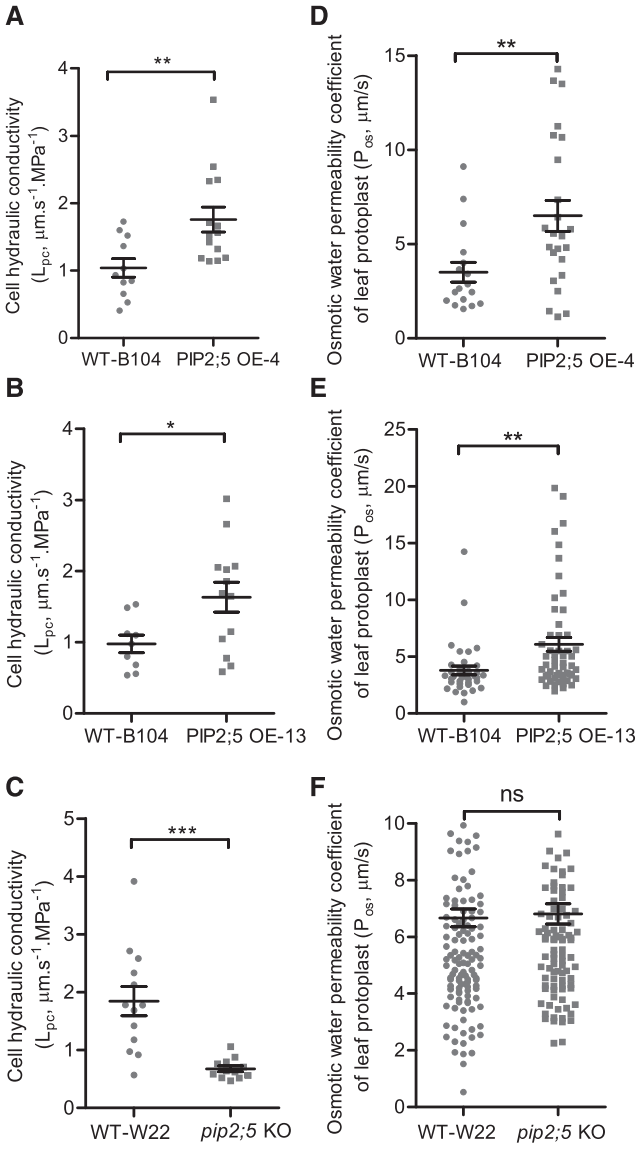


Figure 2. Membrane water permeability of root cortex cells and leaf mesophyll cells. L_{pc} (A–C) and the osmotic water permeability coefficient of leaf mesophyll cell protoplasts (P_{os}; D–F) were measured in wild-type (WT), PIP2;5 OE-4, PIP2;5 OE-13, and *pip2;5* KO lines using 1- and 3-week-old plants, respectively, grown under hydroponic conditions. Individual data dots are shown and data are also expressed as the mean ± SE of 10–15 cells from three to five plants for the L_{pc} and >30 protoplasts from two plants for the P_{os}. Significant differences among the treatments are indicated by $^{*}P < 0.05$, $^{**}P < 0.01$, and $^{***}P < 0.001$. ns, Not significantly different ($P > 0.05$).

regardless of the cell wall hydraulic conductivity, k_w (Fig. 4C, $P < 0.01$). The simulations reproduced the observed contrasts between the PIP2;5 OE and KO lines (Fig. 4, F–H) at the condition where $k_w > 6.9 \times 10^{-10}$ m^2 s^{-1} MPa^{-1} (k_{w2}), and showed that the contribution of PIP2;5 to L_{pc} was saturated in the endodermis and exodermis of wild-type lines (Fig. 4E, $P < 0.05$).

Altered Plant Growth in PIP2;5 Deregulated Plants Under Water-Deficit Conditions

To further investigate the effect of PIP2;5 deregulation on water relations and plant growth, we examined the time course of LER over changes in environmental conditions. During the day, while the evaporative demand increases, hydraulic resistances to water transfer can rapidly decrease the leaf water potential (Ψ_{leaf}) and leaf growth, but this is only observable under suboptimal water conditions (Bouchabké et al., 2006). We therefore measured the leaf water potential and expansion of PIP2;5 OE-4 plants and their wild-type B104

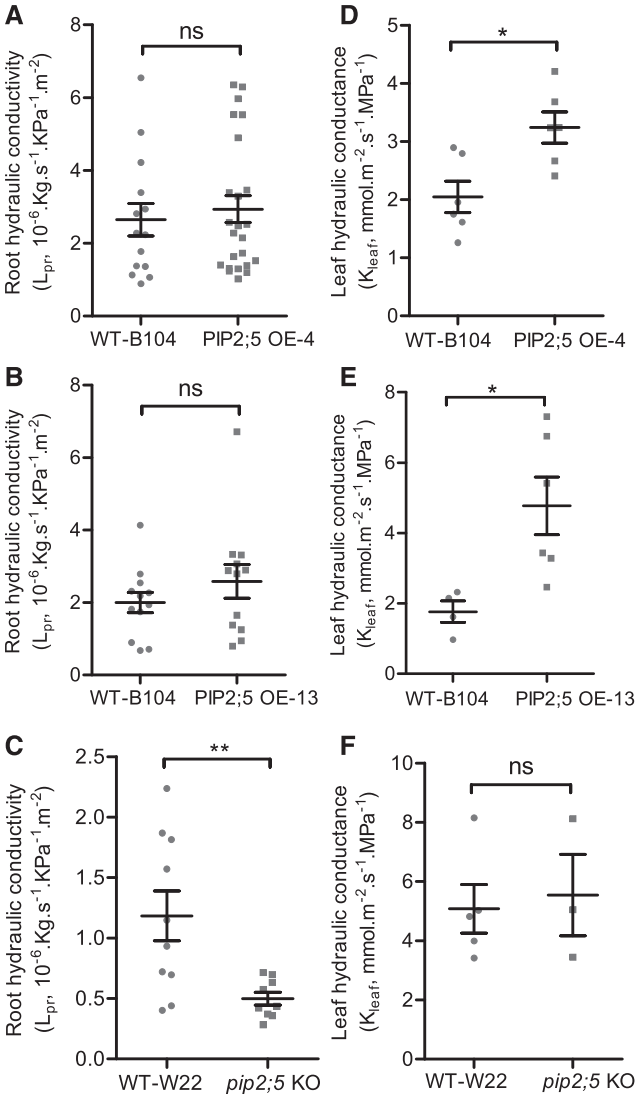


Figure 3. Root hydraulic conductivity and leaf hydraulic conductance. L_{pr} (A–C) and K_{leaf} (D–F) were measured in wild-type (WT), PIP2;5 OE-4, PIP2;5 OE-13, and *pip2;5* KO lines. L_{pr} was measured in 2-week-old maize seedlings and K_{leaf} of newly expanded leaves was measured with 3-week-old plants. Individual data dots are shown and data are also expressed as the mean ± SE of roots and leaves from four to six plants. Significant differences among the treatments are indicated by $^{*}P < 0.05$ and $^{**}P < 0.01$. ns, Not significantly different ($P > 0.05$).

Downloaded from https://academic.oup.com/plphys/article/182/4/2154/6116623 by universite catholique de louvain user on 08 October 2021

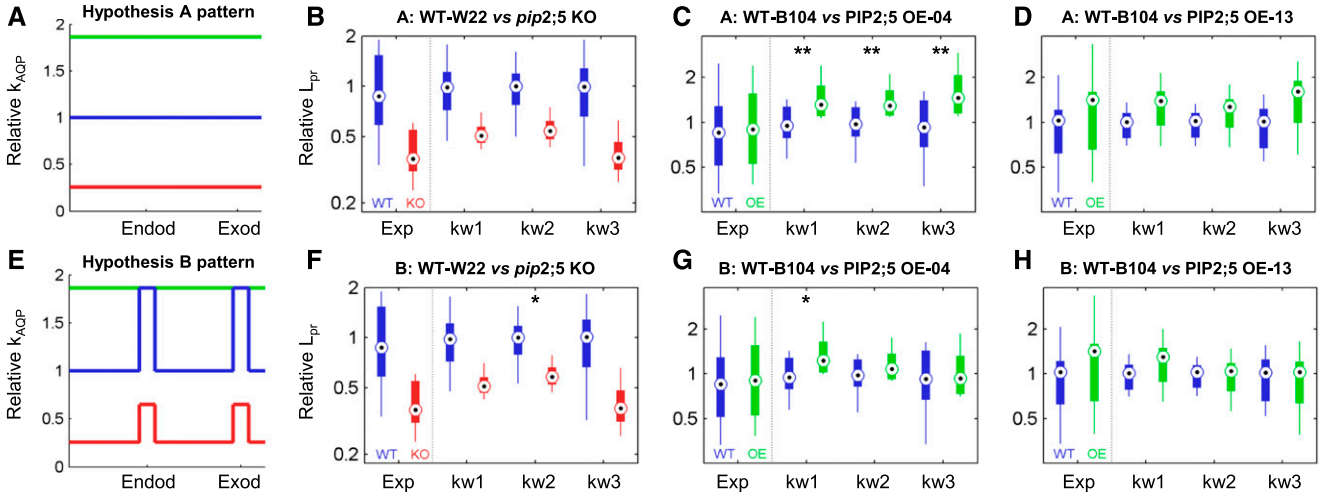


Figure 4. Contrast analysis between experimental and simulated L_{pr} using the MECHA model. Contrast analysis between measured (Exp) and simulated (k_{w1}, k_{w2}, and k_{w3}) L_{pr} in wild-type (WT; blue) and *PIP2;5* deregulated lines (red, *pip2;5* KO; green, PIP2;5 OE; B–D and F–H) for hypothesized radial patterns of plasma membrane permeability ($k_{AQP;}$ A and E). Asterisks indicate significantly different contrasts between measurements and simulations (*$P < 0.05$ and **$P < 0.001$; e.g. in C, contrast between the wild-type and OE lines was larger in simulations than in experiments). Circles and bars indicate the 25th, 50th, and 75th percentiles, and whiskers indicate the most extreme nonoutlier data point.

under well-watered conditions (in order to observe putative intrinsic differences of leaf expansion rate; Fig. 5C) and under moderate water deficit (in order to observe the effects of hydraulics; Fig. 5D).

Under moderate water deficit ($\Psi_{soil} = -0.23$ to -0.26 MPa), we measured a higher leaf water potential in the PIP2;5 OE-4 line than in wild-type B104 plants, while the difference was not observed under well-watered conditions (Fig. 5B). A significantly faster recovery of LER was observed after the early morning drop in PIP2;5 OE-4 compared with wild-type B104 plants, resulting in large differences in LER during the day (Fig. 5D, inset). Overall, the mean LER of PIP2;5 was higher in OE-4 than in wild-type B104 over 1 d (0.75 mm h^{-1} versus 0.40 mm h^{-1}; Supplemental Fig. S5). During the night, the average LER of PIP2;5 OE-4 was 1.42 mm h^{-1} and it was also significantly higher ($P < 0.001$) than the average LER of wild-type B104 (1.05 mm h^{-1}). As expected, these differences were not observed in well-watered conditions (Fig. 5C), indicating that no pleiotropic effects had affected the intrinsic potential LER of OE plants.

A faster recovery of LER was correlated with an increase in PIP aquaporin expression, Ψ_{leaf}, and L_{pr} (Parent et al., 2009; Caldeira et al., 2014a). While no change in L_{pr} was recorded in PIP2;5 OE plants compared with the wild-type B104 plants in well-watered conditions, we compared the L_{pr} in response to short-term osmotic stress (10% [w/v] polyethylene glycol [PEG] 6000; $\Psi = -0.15$ MPa) and observed a higher L_{pr} in PIP2;5 OE-4 than in wild-type B104 plants, though the difference was not significant (Supplemental Fig. S6). These results suggest that the higher root hydraulic conductivity for PIP2;5 OE-4 observed under low osmotic potential translated into differences in leaf water potential and leaf expansion under moderate water deficit, which was not the case under well-watered conditions due to the very low difference in root hydraulic conductivity.

DISCUSSION

A better understanding of the functional role of PIP aquaporins in plant water relations is essential to develop crop lines that use water more efficiently and are more tolerant to water deficit. To this aim, we investigated the direct contribution of PIP2;5, the most expressed PIP aquaporin in maize roots, using reverse genetic approaches. Overexpression of *PIP2;5* under the control of the 35S promoter led to a <2-fold increase in the PIP2;5 protein level in roots, where PIP2;5 is already highly expressed, and an ~10-fold increase in leaves, where PIP2;5 is weakly expressed. This difference in PIP2;5 protein abundance according to the organ suggests the existence of posttranscriptional or posttranslational regulation mechanisms that prevent an excess of PIP2;5 proteins according to the cell type. Different cellular mechanisms modifying PIP abundance in the plasma membrane have been reported (Chaumont and Tyerman, 2014; Maurel et al., 2015) that involve internalization of PIPs from the plasma membrane for degradation and/or recycling. Negative feedback of *PIP* gene transcription could not be excluded either, even though it was not detected by RT-qPCR. The decrease in *PIP2;5* gene expression was obtained using the UniformMu transposon mutated line UFMu00767 (McCarty et al., 2005, 2013; Hunter et al., 2014). In this line, the transposon was inserted in the second intron, leading to an important decrease in mRNA and protein levels. However, a very weak signal for PIP2;5 protein was still

Downloaded from https://academic.oup.com/plphys/article/182/4/2154/6116623 by universite catholique de louvain user on 08 October 2021

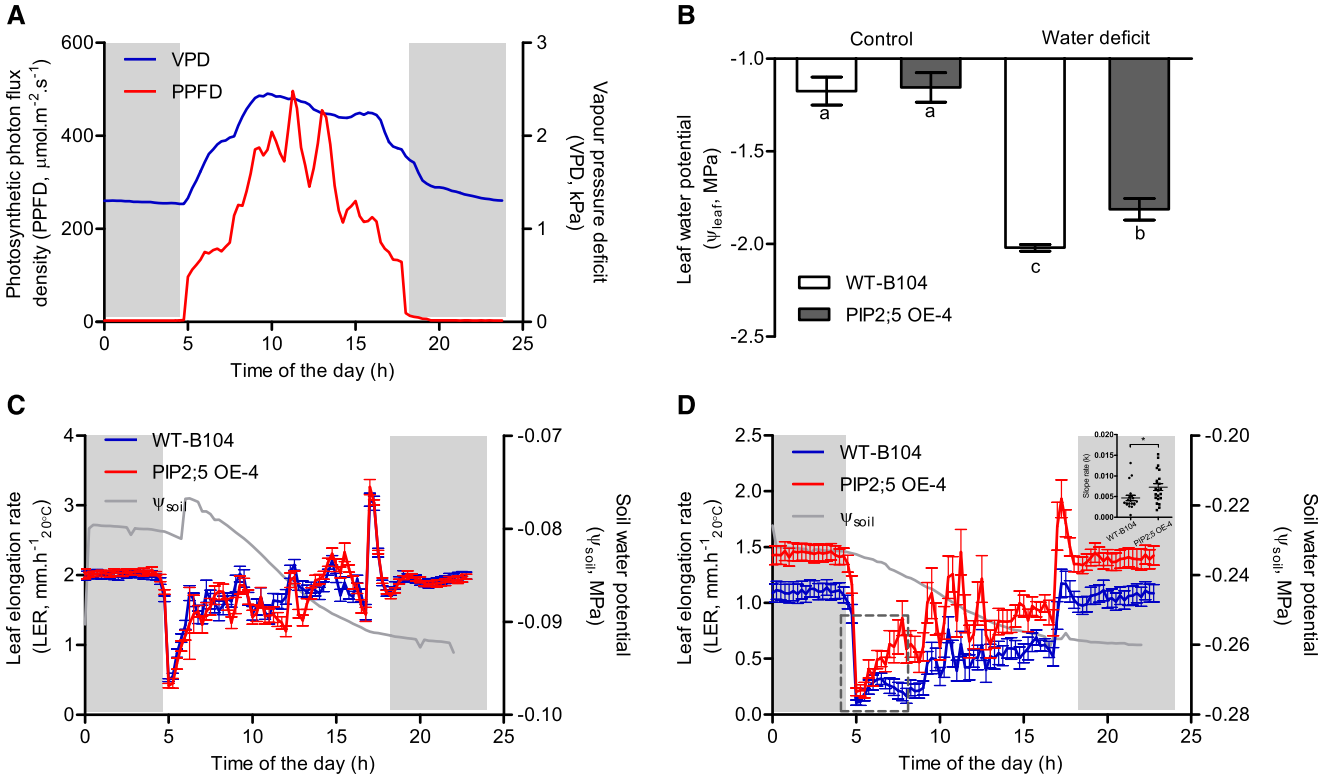


Figure 5. Daily time courses of environmental conditions, leaf water potential, and LER under well-watered and moderate water-deficit treatments. In this experiment, wild-type (WT-B104) and PIP2;5 OE (PIP2;5 OE-4) lines were compared. A, Blue and red traces indicate vapor pressure deficit (VPD) and photosynthetic photon flux density (PPFD), respectively. B, White and gray solid bars show the leaf water potential of wild-type B104 and PIP2;5 OE-4, respectively, under control and water-deficit conditions. One-way ANOVA with Tukey's honestly significant difference (HSD) mean-separation test was used to compare the significant differences between wild-type B104 and PIP2;5 OE-4 plants under control and water-deficit conditions. Significant differences are indicated by lowercase letters ($P < 0.05$). C and D, Blue and red traces show the LERs of wild-type B104 and PIP2;5 OE-4, respectively. Gray traces show the daily soil water potential (Ψ_{soil}). Gray backgrounds represent the sunset period. The slope rate for traces in the dashed square (D) is analyzed in the upper right inset; Student's *t* test was used to determine the significance of difference between wild-type B104 and PIP2;5 OE-4 plants (*$P < 0.05$). LER is expressed per unit thermal time (mm $h^{-1}{}_{20°C}$). Error bars indicate the SE (n = ~3–9 plants).

observed in roots, indicating that the line was not a complete knockout, as demonstrated by RT-qPCR using primers flanking the Mu insertion site to allow the detection of a weak signal in *pip2;5* KO samples (Supplemental Fig. S2).

The cortex cell L_{pc} in intact roots was dependent on PIP2;5 expression levels, with higher and lower values in OE and KO lines, respectively. As no change in the abundance of other PIP aquaporins was detected, this is direct evidence that PIP2;5 facilitated the water diffusion through the cell membranes. We previously showed a correlation between PIP expression and the L_{pc} in roots. The higher abundance of PIPs, including PIP2;5, during the day than during the night, or after a short (8-h) PEG treatment, is correlated with variation in the L_{pc} values (Hachez et al., 2012). Overexpressing or knocking out *PIP* genes in other plant species also results in higher or lower L_{pc}. For instance, in Arabidopsis (*Arabidopsis thaliana*) *pip2;2* KO lines, L_{pc} of the root cortex cells is reduced by ~25% when compared with wild-type plants (Javot et al., 2003). In contrast, L_{pc} is higher in PIP2;5 overexpressing Arabidopsis lines than in the wild type under low temperature (Lee et al., 2012).

While the L_{pr} of *pip2;5* KO plants was significantly decreased, no increase in L_{pr} was recorded in PIP2;5 OE plants under well-watered conditions, indicating that the abundance of PIP2;5 in the root cell membranes is not always correlated to the L_{pr}. The uncorrelated data between PIP abundance, L_{pc}, and L_{pr} was previously observed in maize plants subjected to a short PEG stress, which induces higher PIP expression and a higher L_{pc}, but no change in L_{pr} (Hachez et al., 2012). The composite water transport model (Steudle and Peterson, 1998) assumes that L_{pr} is controlled by the hydraulic conductivity of apoplastic and cell-to-cell pathways in parallel. We proposed that radial variations along each pathway critically affect water transport due to the presence of gatekeeper cells at the beginning (epidermis and exodermis) or the end (endodermis) of the radial

Downloaded from https://academic.oup.com/plphys/article/182/4/2154/6116623 by universite catholique de louvain user on 08 October 2021

path of water (Hachez et al., 2012; Chaumont and Tyerman, 2014). While the current cell pressure probe technology did not allow directly verification of this hypothesis, the use of the quantitative modeling framework MECHA (Couvreur et al., 2018) gave us the opportunity to get a better understanding of the mechanisms involved. A statistical comparison of our measured and simulated L_{pr} results largely supports the hypothesis that plasma membrane permeability is not radially uniform in the wild type (hypothesis A rejected; $P < 0.01$; Fig. 4C) but may be saturated in the endodermis and exodermis (hypothesis B; Fig. 4E), thus following the observed radial aquaporin expression patterns observed by Hachez et al. (2006a). This is an important result, as none of the models of radial water flow, from the simplest to the most sophisticated, accounts for such heterogeneity, which does affect L_{pr} in the wild type. On the other hand, knocking out *PIP2;5* gene expression led to a decrease in L_{pr}, suggesting that PIP2;5 is an essential actor facilitating radial water flow and controlling whole root conductivity, as also observed in our simulations. Quantification of the level of active PIP2;5 proteins in the endodermis would be very informative. Indeed, *PIP2;5* gene OE in this specific cell type would not lead to an increase in PIP2;5 protein due to the above-mentioned posttranslational mechanisms and the fact that a maximum of active PIP2;5 (and other PIPs) was already reached. These predictions could be refined by generating maize lines with deregulated PIP expression exclusively in the endodermis or the exodermis.

Maize lines expressing *PIP2;5* complementary DNA (cDNA) under the control of *p35*S promoter showed a much higher increase in PIP2;5 protein abundance in leaves than in roots. Considering that general PIP expression in maize is lower in leaves than in roots and that *PIP2;5* is very weakly expressed in leaves (Hachez et al., 2006a, 2008; Heinen et al., 2009), we hypothesize that overexpressing PIP2;5 in this organ was not limited by similar posttranscriptional or posttranslational mechanisms observed in roots. Similar to what was observed in root cells, an increase in P_{os} was measured for the leaf mesophyll cells overexpressing PIP2;5. We previously demonstrated that transient expression of PIP2;5 in mesophyll cells increases the water membrane permeability (Besserer et al., 2012). However, in contrast to the effect of PIP2;5 OE on the whole root conductance, OE of PIP2;5 led to a higher K_{leaf} compared to that of wild-type B104 plants (Fig. 3, D and E). A similar result was found, for instance, in tomato (*Solanum lycopersicum*) plants overexpressing NtAQP1 (Sade et al., 2010). Inversely, down-regulation of *PIP1* gene expression in Arabidopsis plants results in a decrease in the mesophyll cell P_{os} and the K_{leaf} (Sade et al., 2014). K_{leaf} and leaf radial water flow are thought to be mainly controlled by the vascular bundle sheath cells surrounding the veins (Hachez et al., 2006a; Sack and Holbrook, 2006; Shatil-Cohen et al., 2011; Buckley, 2015). These cells can have suberized walls, and are associated with a very low apoplastic flow. Arabidopsis plants, in which *PIP1* genes are specifically silenced in vascular bundle sheath cells, also exhibit decreased mesophyll and bundle sheath P_{os} and decreased K_{leaf} (Sade et al., 2014). In our work, PIP2;5 OE plants exhibited higher P_{os} of the mesophyll cells and possibly also of the bundle sheath cells, resulting in an enhancement of conductance in the bundle sheath, mesophyll cells, and K_{leaf}. The observation that no difference in P_{os} and K_{leaf} was observed in *pip2;5* KO plants was expected, since PIP2;5 is weakly expressed in leaf tissues (Hachez et al., 2008). Extending the MECHA model to leaf tissues and cells will be very useful in addressing these questions related to leaf water relations.

LER is controlled by plant hydraulic properties, including leaf and xylem water potential, transpiration, and root hydraulic conductivity (Caldeira et al., 2014a), and involves hormonal regulation (Nelissen et al., 2012, 2018; Avramova et al., 2015). Actually, we considered that short-term variation of LER is a proxy for the change of xylem water potential (Parent et al., 2009; Caldeira et al., 2014a). In a mild water deficit, a faster recovery of LER after the early morning drop, and a higher LER during the day and night, were recorded in PIP2;5 OE-4 compared with wild-type B104 plants. This LER response in PIP2;5 OE plants can be correlated with a higher K_{leaf} and is consistent with the effect of K_{leaf} on LER recovery observed in transgenic plants that differ in abscisic acid concentration in the xylem sap, showing differences in the L_{pr} (Parent et al., 2009). Interestingly, while wild-type B104 and PIP2;5 OE plants had a similar L_{pr} in well-watered conditions, an osmotic stress led to an increased L_{pr} in the OE plants, suggesting that changes in hydraulic conductance (L_{pr} and K_{leaf}) by PIP2;5 deregulation at the cell level translated into an overall change in whole-plant hydraulic fluxes (and leaf water potential) that affects the LER in mild-stress conditions. The observation that the LER was not affected in well-watered plants implies that molecular mechanisms controlling overall root hydraulic conductance occur in some cell types, resulting in a non-uniform distribution of water permeability or at specific positions along the root axis (e.g. the connection between root and leaf xylems).

In conclusion, deregulation of PIP2;5 aquaporin expression in maize plants highlighted their role in controlling the root and leaf cell water permeability. However, understanding the results obtained at the root level required a hydraulic model developed at the cell and tissue scales. MECHA allowed us to discard the hypothesis of radially uniform L_{pc}, and it suggests that in well-watered conditions, the gatekeeper cells of wild-type plants have a saturated membrane permeability. Transposing the model to the aerial part will definitely offer possibilities to better understand the hydraulic properties of tissues and cells in diverse conditions and investigate the role and regulation of aquaporins in specific hydraulic processes. Indeed, we showed that the increase in hydraulic conductance by overexpressing aquaporin positively affects the LER under moderate stress conditions.

Downloaded from https://academic.oup.com/plphys/article/182/4/2154/6116623 by universite catholique de louvain user on 08 October 2021

MATERIALS AND METHODS

Plasmids and Genetic Construction to Generate PIP2;5 OE Lines

The cauliflower mosaic virus *p35S* promoter was PCR amplified from the pMDC43 vector (Curtis and Grossniklaus, 2003) and cloned into the Gateway entry vector pDONR P4-P1R (Invitrogen) according to the manufacturer's instructions. The *YFP* cDNA followed by the *tnos* terminator sequence were amplified together from the pH35GY vector (Kubo et al., 2005) and cloned into the pDONR221 vector. Finally, a uracil-excision based cloning cassette (USER) was added downstream of the *p35S* promoter sequence and subsequently cloned into pDONR P2R-P3 (Nour-Eldin et al., 2006; Hebelstrup et al., 2010). These three entry vectors were verified by sequencing and their inserts brought together by *attR* and *attL* site recombination into the pBb7m34GW backbone vector suitable for maize (*Zea mays*) transformation (Karimi et al., 2013; https://gateway.psb.ugent.be). The latter contains the *bar* selectable gene under control of the *p35S* promoter, which induces resistance to the herbicide bialaphos and allows selection of transformed calli and shoots using phosphinotricin-containing media. The cDNA encoding ZmPIP2;5 was PCR amplified using USER primers (forward primer, 5′ GGTCTTAAUATGGCCAAGGACATCGA GG 3′; reverse primer, 5′ GGCATTAAUCTAGCGGCTGAAGGAGGCA 3′) and inserted into the destination vector to obtain the final vector. This plasmid was used to transform the hypervirulent EHA101 *Agrobacterium tumefaciens* strain (Hood et al., 1986) by heat shock and subsequently used for transformation of maize immature embryos from the B104 inbred line according to the method described by Coussens et al. (2012), in collaboration with the Maize Transformation platform of the Center for Plant Systems Biology (VIB-Ghent University, Ghent, Belgium). Briefly, immature embryos were isolated from ears 12 to 14 d after fertilization and cocultivated with EHA101 *A. tumefaciens* strain carrying the plasmid of interest for 3 d in the dark at 21°C. After cocultivation, immature embryos were cultivated for 1 week without selection, followed by a 4-month period of subculturing on selective media containing increasing amounts of phosphinotricin (starting from 1.5 to 6 mg/L) to select transformed embryogenic calli in dark conditions at 25°C. After selection, the embryogenic calli were transferred to bigger containers and placed in a growth chamber (24°C, 55 μE m^{-2} s^{-1} light intensity, 16 h/8 h day/night regime) for transgenic T0 shoot/plantlet formation in vitro. Eleven rooted transgenic T0 plants selected from independently transformed immature embryos tested positive for the phosphinotricin acetyltransferase (PAT) enzyme (encoded by the *bar* selectable marker gene) using the TraitChek Crop and Grain Test Kit (Strategic Diagnostics). The presence of the transgenic *ZmPIP2;5* cDNA insertion was also confirmed by PCR amplification of genomic DNA using the *p35S* forward primer (5′ CCACTATCCTTCGCAAGACCC 3′) and *T35S* reverse primer (5′ GGTGATTTTTGCGGACTCTAGCAT 3′). The transgenic T0 plants were transferred to soil and kept for 1 month in a growth chamber (16 h/8 h day/night regime at 24°C, 55 μmol m^{-2} s^{-1} light intensity, and 55% relative humidity) in 1 L pots for acclimation, and then moved to a greenhouse (26°C/22°C day/night temperature, 300 μmol m^{-2} s^{-1} light intensity under a 16 h/8 h day/night regime) and 10 L pots until flowering. A backcross with the B104 genotype was performed by pollinating either ears of T0 plants with B104 pollen or B104 ears with T0 plants pollen. The ears were then harvested 4 weeks after fertilization and dried for several weeks at 25°C before sowing the segregating T1 generation. The T2 generation was generated by backcross between B104 and the heterozygous T1 plant in the greenhouse. T1- and T2-generation heterozygous plants segregating for the *ZmPIP2;5* transgene (PIP2;5 OE) and nontransgenic siblings (wild-type B104) were used in this study. Finally, two independent OE lines (PIP2;5 OE-4 and PIP2;5 OE-13) with high ZmPIP2;5 protein content in western blotting analysis were used for all further measurements.

pip2;5 KO Line

The *pip2;5* KO line (UFMu00767), generated from the W22 inbred line, was found in MaizeGDB (https://maizegdb.org/) and obtained from Uniform Mu stocks in Maize Genetics Cooperation Stock Center (http://maizecoop.cropsci.uiuc.edu/). To confirm the Mu transposon insertion in *PIP2;5* gene, genomic DNA was extracted from the second leaf of a 1-week-old maize seedling, with TPS extraction buffer (100 mM Tris-HCl, pH 8.0, 10 mM EDTA, and 1 M KCl). PCR was performed using a Mu-TIR specific forward primer (Mu-Terminal Inverted Repeat, TIR6: 5′ AGAGAAGCCAACGCCAWCGCCTCYATTTCGTC 3′; McCarty et al., 2013) and *PIP2;5* specific reverse primer (5′ CGTCTACAC CGTCTTCTCCG 3′) to detect the Mu insertion, and with *PIP2;5* specific primers (forward, 5′ AGGCAGACGATCCCAGCTT 3′; reverse, 5′ CGTCTACAC CGTCTTCTCCG 3′) to detect the *PIP2;5* gene. Heterozygous plants were self-pollinated and a segregation ratio of 1:2:1 wild-type W22:heterozygous:homozygous seeds was obtained. The wild-type W22 and homozygous plants were used for the measurements.

Growth Conditions

Hydroponic culturing was conducted to obtain plant material for the measurements of cell hydraulic conductivity, root hydraulic conductivity, and leaf hydraulic conductance. Maize seeds were surface sterilized using 2% (w/v) NaClO solution for 5 min, rinsed with distilled water, and placed between two wet tissue papers in a square petri dish (Greiner Bio-One). The seeds were put in the dark at 30°C for 72 h. After germination, the seedlings were transferred to a 2 L beaker with one-half strength nutrient solution [1.43 mM $Ca(NO_3)_2 0.4H_2O$, 0.32 mM KH_2PO_4, 0.35 mM K_2SO_4, 1.65 mM $MgSO_4 0.7H_2O$, 9.1 μM $MnCl_2 0.4H_2O$, 0.52 μM $(NH_4)_6Mo_7O_{24} 0.4H_2O$, 18.5 μM H_3BO_3, 0.15 μM $ZnSO_4 0.7H_2O$, 0.16 μM $CuSO_4 0.5H_2O$, and 35.8 μM Fe-EDTA]. The nutrient solution pH was adjusted to 5.5 and replaced every 2 d. The nutrient solution was aerated with the aid of aquarium diffusers. After 1 week, the full-strength nutrient solution was used until the end of experiments. The plants were grown in a growth chamber on a 16 h/8 h light/dark cycle (25°C/18°C) and a daytime light intensity of 200 μmol m^{-2} s^{-1} at the top of the leaf level.

Soil culturing was conducted in the growth chamber or in the greenhouse. Maize seeds were surface sterilized using 2% (w/v) NaClO solution for 5 min, rinsed with distilled water, and placed in Jiffypots (6 cm diameter) filled with 80% (v/v) potting soil (DCM) and 20% (v/v) vermiculite (Agra-vermiculite). After 2 weeks, the seedlings were transferred to 2 L pots (MCl 17, Pöppelmann) filled with the same substrate and vermiculite. After another 4 weeks, the plants were transferred to 10 L pots (MCl 29, Pöppelmann).

Protein Extraction and Western Blot

Microsomal membrane fractions were prepared as described by Hachez et al. (2006), with a few modifications. Briefly, leaf (newly expanded leaf) or root (primary root) tissues from 1-week-old maize seedlings were flash-frozen in liquid nitrogen in aluminum foil and ground with mortar and pestle using 2 mL of extraction buffer (250 mM sorbitol, 50 mM Tris-HCl, pH 8, and 2 mM EDTA) containing freshly added 0.6% (w/v) polyvinyl pyrrolidone K30, 1 mM phenylmethanesulfonate, and 0.5 mM dithiothreitol, supplemented with 2 μg mL^{-1} of protease inhibitors (leupeptin, aprotinin, antipain, pepstatin, and chymostatin). Debris were removed with a first centrifugation at 770*g* at 4°C for 10 min and the subsequent supernatant was centrifuged at 10,000*g* at 4°C for 10 min. The supernatant was then centrifuged at 54,000*g* at 4°C for 30 min and the resulting pellet (microsomal fraction) was resuspended in 50 μL of suspension buffer (330 mM Suc, 5 mM KH_2PO_4, and 3 mM KCl, pH 7.8) and sonicated twice for 5 s. Total protein concentration was determined by the Bradford protein assay (Bradford, 1976).

Twenty micrograms (root) and 30 μg (leaf) of total proteins were mixed with 6× Laemmli buffer (240 mM Tris-HCl, pH 6.8, 6% [w/v] SDS, 30% [w/v] glycerol, and 0.05% [w/v] bromophenol blue) and freshly added 10% (w/v) dithiothreitol, in a total volume of 45 μL. They were solubilized for 10 min at 60°C and loaded in 12% (w/w) acrylamide gels (Eurogentec) for separation by electrophoresis (120 V for ~1 h). After transfer to a polyvinylidene fluoride membrane (Trans-Blot Turbo Mini PVDF Transfer Packs, Biorad), the proteins were immunodetected using antisera raised against the amino-terminal peptides of ZmPIP1;2, ZmPIP2;1/2;2, and ZmPIP2;5 (Hachez et al., 2006a, 2012). The antibody raised against H^+-ATPase (PMA; Morsomme et al., 1996) was used as a control to normalize the protein level. The blotting signal was detected using an Amersham imager 600 (GE Healthcare). The signal was quantified with ImageJ software (National Institutes of Health; http://rsb.info.nih.gov/ij) and normalized with the signal of PMA.

RNA Extraction and RT-qPCR

One-week-old maize seedlings were used for RNA extraction and RT-qPCR. The whole newly expanded leaf and primary root were harvested and immediately frozen in liquid nitrogen, and the samples were stored at −80°C until RNA extraction. RNA extraction was performed with the Spectrum Plant Total RNA Kit (Sigma-Aldrich) according to the manufacturer's instructions. DNAse I (Sigma-Aldrich) digestion was performed directly on the column during RNA

Downloaded from https://academic.oup.com/plphys/article/182/4/2154/6116623 by universite catholique de louvain user on 08 October 2021

extraction according to the manufacturer's recommendations. The RNA concentrations and the quality of each sample were measured with a Nanodrop ND-1000 (Isogen Life Science), and 1.5 μg of total RNA was used for reverse transcription and the cDNA synthesis was performed with the Moloney Murine Leukemia Virus Reverse Transcriptase (M-MLV RT) kit (Promega) according to the manufacturer's instructions. RT-qPCR was performed in 96-well plates using a StepOnePlus Real-Time PCR System (Life Technologies) in a volume of 20 μL containing 10 μL of RT-qPCR Mastermix Plus for SYBR Green I (Eurogentec), 1 μL of forward and reverse primers (Supplemental Table S1), 1 μL cDNA, and 7 μL DEPC-water. The PCR cycle program was 2 min at 50°C and 10 min at 95°C for DNA polymerase activation, and 40 cycles of 15 s at 95°C and 60 s at 60°C. The $2^{-\Delta Ct}$ method was used to analyze the relative expression of six *ZmPIP1s* (*ZmPIP1–ZmPIP1;6*) and six *ZmPIP2s* (*ZmPIP2;1–ZmPIP2;6*). Three reference genes, *ACT1*, *EF1-α*, and *polyubiquitin*, were used to normalize the expression.

Cell Pressure Probe Measurement

One-week-old maize seedlings were used for cell pressure probe measurements, according to the methods of Hachez et al. (2012) and Volkov et al. (2006). Briefly, the plant and primary root was maintained in a petri dish containing the nutrient solution, and the root region near to the last lateral root (5–7 cm near the root tip) was measured. Cell turgor pressure (P), $T_{1/2}$, and pressure change value (ΔP) were recorded. These parameters were measured for three to five cells from each plant, and three to five plants were analyzed. After the measurements, average values of cell volume and cell surface area were calculated through microscopic analyses of 7–30 cells from the third to the sixth cell layer taken at 5–7 cm from the root tip. Cell osmotic pressure was checked with a micro-osmometer (model 3300, Advanced Instruments). In this study, a cell osmotic pressure of 0.88 MPa was used for all calculations. Cell elastic modulus (ε) and cell hydraulic conductivity (L_{pc}) were calculated according to Volkov et al. (2006).

L_{pr} and K_{leaf} Measurement

Three-week-old maize plants growing in a phytotron were used for (L_{pr} measurements, according to the methods of Ding et al. (2015). In the phytotron, the light cycling was from 06:00 to 22:00. In the morning, between 09:00 and ~11:00 (measurements beginning 3 h after light onset), the primary root was cut and connected to an HCFM (Decagon Devices). The connection was performed as quickly as possible (1 or 2 min, or less) to minimize the effect of the root excision on the L_{pr}, as previously reported Vandeleur et al. (2014). A transient method was used to record the value change of the flow rate (F) and applied pressure (Pi), and the slope rate (Kr, given in kilograms per second per megapascal) was analyzed between the correlation of F and Pi. For one root, three to five replications were performed for the measurement. After the measurement, the primary root was scanned with an Epson perfection V33 scanner and the root surface area was analyzed with ImageJ (National Institutes of Health; http://rsb.info.nih.gov/ij). Then the Kr was normalized with the root surface area for the L_{pr} calculation. For PEG-treated plants, 10% (w/v) PEG-6000 was added to the nutrient solution in hydroponic culture, and L_{pr} was measured after 2 and 4 h.

K_{leaf} was measured between 13:00 and ~15:00 (measurements beginning 7 h after light onset) with a HCFM (Tyree et al., 2005; Ferrio et al., 2012) using 3-week-old maize plants. The newly expanded leaf was cut with the leaf sheath, and wrapped around a plastic stick covered by UHUpatafix (UHU). Then a tape of polytetrafluoroethylene film was wrapped around the leaf sheath. Afterward, the leaf sheath was excised under water and connected with the HCFM. Approximately 0.2 MPa pressure was applied in the system and a quasi-steady state method was used to record the flow rate and conductance every 8 s for 10–30 min until the conductance was constant. During the measurement, the leaf was immersed in water to stop transpiration. After the measurement, the leaf was scanned with Epson perfection V33 scanner (Epson) and the leaf area was analyzed with ImageJ software. The hydraulic conductance was normalized with the leaf area to calculate K_{leaf}.

Protoplast Swelling Assay

Leaf mesophyll protoplasts were isolated from newly expanded leaves of 3-week-old maize plants, and a swelling assay was performed according to the methods of Moshelion et al. (2004) and Shatil-Cohen et al. (2014). The leaf abaxial side was scratched with a glass paper, and then the leaf was cut into small sections and transferred to the digestion buffer with the scratched side in contact with the buffer (0.6% [w/v] cellulose R10 [Duchefa Biochemine], 0.1% [w/v] pectolyase [Sigma-Aldrich], 0.3% [w/v] Macerozyme R10 [Duchefa Biochemine], 5 mg mL^{-1} bovine serum albumin, and 5 mg mL^{-1} polyvinyl pyrrolidone K30). The analysis of the osmotic water permeability coefficient was based on the methods of Shatil-Cohen et al. (2014).

LER Measurement

Leaf growth was measured in the high-throughput phenotyping platform Phenodyn (Sadok et al., 2007) of the LEPSE laboratory in Montpellier (https://www6.montpellier.inra.fr/*lepse/M3P*). Plants were grown in one PVC column filled with clay balls, which makes it possible to tare columns at 1.2 kg. Then, columns were filled with 4.4 kg of a mix of loam (5% to 10% [v/v]) and soil. Plants were watered daily with nutritive solution. Sampling of the newest leaf was carried out at the four-leaf stage and PCR was performed to characterize the transgenic PIP2;5 OE plants. After the characterization, three plants were kept in the column, including either three wild-type B104 or three PIP2;5 OE plants or a mix of the two (either two wild-type B104 or two PIP2;5 OE) for the LER measurement. Plants were grown under a 14 h light/10 h dark cycle at 19°C to 26°C (day, minimum to maximum)/19°C to 21°C (night, minimum to maximum) in a greenhouse. Well-watered conditions were kept until plants reached the four-leaf developmental stage. Then a progressive water deficit was applied. Each pot was placed on a scale with automated irrigation to impose the targeted soil water potential. LER was measured when the tip of the sixth leaf appeared above the whorl and lasted until the appearance of leaf 8. LER was expressed in thermal time, via equivalent days at 20°C according to Parent et al. (2010). Ψ_{leaf} was measured in a pressure chamber between 12:00 and 14:00 in the greenhouse with nonexpanding leaves.

Inference on Radial Patterns of Cell Membrane Permeability

In order to test hypotheses about the radial pattern of plasma membrane permeability, we simulated how measured cell-scale permeability (L_{pc}) translates into L_{pr} for each pattern, and compared the distributions of simulated and measured L_{pr}.

Assuming that the axial resistance to water flow is negligible, the simulation framework MECHA (Couvreur et al., 2018) estimates L_{pr} from root transverse anatomy and subcellular-scale hydraulic properties. In order to plug the measured L_{pc} into the model, we partitioned it into its two main components: the plasma membrane hydraulic conductivity (k_{AQP}, including the contribution of aquaporins) and the conductance of plasmodesmata per unit membrane surface (k_{PD}). The latter parameter was assumed to equal 2.4×10^{-7} m s^{-1} MPa^{-1}, according to the methods of Couvreur et al. (2018), based on plasmodesmata frequency data from Ma and Peterson (2001) and the low range of plasmodesmata conductance estimated by Bret-Harte and Silk (1994). This value was subtracted from the measured L^{pc} to obtain k_{AQP}. As the value of the cell wall k_w is highly uncertain, a range of low ($k_{w1} = 6.9 \times 10^{-11}$ m^2 s^{-1} MPa^{-1}), medium ($k_{w2} = 6.9 \times 10^{-10}$ m^2 s^{-1} MPa^{-1}), and high ($k_{w3} = 1.4 \times 10^{-8}$ m^2 s^{-1} MPa^{-1}) values were tested. Finally, the hydrophobic wall segments of Casparian strips in the endodermis and exodermis were attributed to null hydraulic conductivity. As experimental observations confirmed that root anatomy only varied slightly between the tested lines, the same geometrical layout was used for all of them, except for the mutant PIP2;5 OE-13 line, whose cell sizes were multiplied by 1.17, as observed experimentally. The anatomy was representative of a maize primary root (0.9 mm diameter), 5 cm proximal to the tip (for details, see Couvreur et al., 2018). In the future, it will be possible to generate anatomies more representative of each mutant with the tool GRANAR (Heymans et al., 2019).

In hypothesis A we assumed that k_{AQP} is radially uniform and equal to that measured in cortical cells of wild-type, PIP2;5 OE, and *pip2;5* KO lines (Fig. 4A). In hypothesis B, we assumed that while k_{AQP} uniformly saturates in the PIP2;5 OE lines, it also saturates in the endodermis and exodermis of the wild type (Fig. 4E). In addition, in this hypothesis we also assumed that since PIP2;5 is not the only aquaporin highly expressed in the endodermis and exodermis, these cell layers may retain k_{AQP} values as high as half of the saturated values in the *pip2;5* KO line (Fig. 4E).

L_{pr} values were estimated with MECHA for each combination of measured L_{pc} (10–14 repetitions) by hypothesized radial pattern (2), by wild-type or PIP2;5 deregulated lines (6), or by cell wall hydraulic conductivity value (3).

Downloaded from https://academic.oup.com/plphys/article/182/4/2154/6116623 by universite catholique de louvain user on 08 October 2021

Relative L_{pr} was calculated by dividing the L_{pr} in the wild-type and associated deregulated lines by the average L_{pr} of the wild-type line. A lognormal transformation was applied to the relative L_{pr} to correct for the skewness of their distributions in the following statistical analyses. Contrasts between measured and simulated relative L_{pr} in the wild-type and associated deregulated lines were then investigated with ANOVA2 functions in the software SAS (SAS Institute). The contrast between the measured L_{pr} in the wild-type and PIP2;5 deregulated lines was considered significantly different from the contrast between simulated L_{pr} in wild-type and deregulated lines starting at a *P*-value of 0.05.

Statistical Analysis

Student's *t* test was applied to determine the significance of differences of average values between the PIP2;5 OE/KO lines and their respective wild-type plants. In Figures 4 and 5B, one-way ANOVA with Tukey's honestly significant difference (HSD) mean-separation test was used to compare leaf water potential between wild-type B104 and PIP2;5 OE-4 plants under control and water deficit conditions.

Accession Numbers

All accession numbers of the genes are listed in Supplemental Table S2.

Supplemental Data

The following supplemental materials are available.

Supplemental Figure S1. Levels of *PIP* transcripts in roots and leaves of wild-type, PIP2;5 OE-4, PIP2;5 OE-13, and *pip2;5* KO lines.

Supplemental Figure S2. RT-PCR amplification of *PIP2;5*.

Supplemental Figure S3. Comparison of PIP1;2 and PIP2;1/2;2 protein levels in wild-type B104 and PIP2;5 OE lines or wild-type W22 and *pip2;5* KO lines.

Supplemental Figure S4. Localization and expression of PIP2;5 in the W22 line.

Supplemental Figure S5. Mean LER during the night and day.

Supplemental Figure S6. Comparison of L_{pr} between wild-type B104 and the PIP2;5 OE-4 line under control and PEG treatments.

Supplemental Table S1. Primers used for the RT-qPCR experiments.

Supplemental Table S2. Accession numbers of the genes.

ACKNOWLEDGMENTS

We thank Lucie Bugeia for her help in performing the LER measurement in the *Phenodyn* platform.

Received November 20, 2019; accepted January 6, 2020; published January 24, 2020.

LITERATURE CITED

Avramova V, Sprangers K, Beemster GTS (2015) The maize leaf: Another perspective on growth regulation. Trends Plant Sci **20:** 787–797

Besserer A, Burnotte E, Bienert GP, Chevalier AS, Errachid A, Grefen C, Blatt MR, Chaumont F (2012) Selective regulation of maize plasma membrane aquaporin trafficking and activity by the SNARE SYP121. Plant Cell **24:** 3463–3481

Bouchabké O, Tardieu F, Simonneau T (2006) Leaf growth and turgor in growing cells of maize (*Zea mays* L.) respond to evaporative demand under moderate irrigation but not in water-saturated soil. Plant Cell Environ **29:** 1138–1148

Bradford MM (1976) A rapid and sensitive method for the quantitation of microgram quantities of protein utilizing the principle of protein-dye binding. Anal Biochem **72:** 248–254

Bret-Harte MS, Silk WK (1994) Nonvascular, symplasmic diffusion of sucrose cannot satisfy the carbon demands of growth in the primary root tip of *Zea mays* L. Plant Physiol **105:** 19–33

Buckley TN (2015) The contributions of apoplastic, symplastic and gas phase pathways for water transport outside the bundle sheath in leaves. Plant Cell Environ **38:** 7–22

Caldeira CF, Bosio M, Parent B, Jeanguenin L, Chaumont F, Tardieu F (2014a) A hydraulic model is compatible with rapid changes in leaf elongation under fluctuating evaporative demand and soil water status. Plant Physiol **164:** 1718–1730

Caldeira CF, Jeanguenin L, Chaumont F, Tardieu F (2014b) Circadian rhythms of hydraulic conductance and growth are enhanced by drought and improve plant performance. Nat Commun **5:** 5365

Chaumont F, Tyerman SD (2014) Aquaporins: Highly regulated channels controlling plant water relations. Plant Physiol **164:** 1600–1618

Coussens G, Aesaert S, Verelst W, Demeulenaere M, De Buck S, Njuguna E, Inzé D, Van Lijsebettens M (2012) Brachypodium distachyon promoters as efficient building blocks for transgenic research in maize. J Exp Bot **63:** 4263–4273

Couvreur V, Faget M, Lobet G, Javaux M, Chaumont F, Draye X (2018) Going with the flow: Multiscale insights into the composite nature of water transport in roots. Plant Physiol **178:** 1689–1703

Curtis MD, Grossniklaus U (2003) A gateway cloning vector set for high-throughput functional analysis of genes in planta. Plant Physiol **133:** 462–469

Ding L, Gao C, Li Y, Li Y, Zhu Y, Xu G, Shen Q, Kaldenhoff R, Kai L, Guo S (2015) The enhanced drought tolerance of rice plants under ammonium is related to aquaporin (AQP). Plant Sci **234:** 14–21

Ferrio JP, Pou A, Florez-Sarasa I, Gessler A, Kodama N, Flexas J, Ribas-Carbó M (2012) The Péclet effect on leaf water enrichment correlates with leaf hydraulic conductance and mesophyll conductance for CO_2. Plant Cell Environ **35:** 611–625

Fetter K, Van Wilder V, Moshelion M, Chaumont F (2004) Interactions between plasma membrane aquaporins modulate their water channel activity. Plant Cell **16:** 215–228

Foster KJ, Miklavcic SJ (2017) A comprehensive biophysical model of ion and water transport in plant roots. I. Clarifying the roles of endodermal barriers in the salt stress response. Front Plant Sci **8:** 1326

Grondin A, Rodrigues O, Verdoucq L, Merlot S, Leonhardt N, Maurel C (2015) Aquaporins contribute to ABA-triggered stomatal closure through OST1-mediated phosphorylation. Plant Cell **27:** 1945–1954

Hachez C, Heinen RB, Draye X, Chaumont F (2008) The expression pattern of plasma membrane aquaporins in maize leaf highlights their role in hydraulic regulation. Plant Mol Biol **68:** 337–353

Hachez C, Moshelion M, Zelazny E, Cavez D, Chaumont F (2006a) Localization and quantification of plasma membrane aquaporin expression in maize primary root: A clue to understanding their role as cellular plumbers. Plant Mol Biol **62:** 305–323

Hachez C, Veselov D, Ye Q, Reinhardt H, Knipfer T, Fricke W, Chaumont F (2012) Short-term control of maize cell and root water permeability through plasma membrane aquaporin isoforms. Plant Cell Environ **35:** 185–198

Hachez C, Zelazny E, Chaumont F (2006b) Modulating the expression of aquaporin genes in planta: A key to understand their physiological functions? Biochim Biophys Acta **1758:** 1142–1156

Hebelstrup KH, Christiansen MW, Carciofi M, Tauris B, Brinch-Pedersen H, Holm PB (2010) UCE: A uracil excision (USER)-based toolbox for transformation of cereals. Plant Methods **6:** 15

Heinen RB, Bienert GP, Cohen D, Chevalier AS, Uehlein N, Hachez C, Kaldenhoff R, Le Thiec D, Chaumont F (2014) Expression and characterization of plasma membrane aquaporins in stomatal complexes of *Zea mays*. Plant Mol Biol **86:** 335–350

Heinen RB, Ye Q, Chaumont F (2009) Role of aquaporins in leaf physiology. J Exp Bot **60:** 2971–2985

Heymans A, Couvreur V, LaRue T, Paez-Garcia A, Lobet G (2019) GRANAR, a new computational tool to better understand the functional importance of root anatomy. bioRxiv 645036 doi:10.1101/645036

Hood EE, Helmer GL, Fraley RT, Chilton MD (1986) The hypervirulence of *Agrobacterium tumefaciens* A281 is encoded in a region of pTiBo542 outside of T-DNA. J Bacteriol **168:** 1291–1301

Hunter CT, Suzuki M, Saunders J, Wu S, Tasi A, McCarty DR, Koch KE (2014) Phenotype to genotype using forward-genetic Mu-seq for

Downloaded from https://academic.oup.com/plphys/article/182/4/2154/6116623 by universite catholique de louvain user on 08 October 2021

identification and functional classification of maize mutants. Front Plant Sci **4:** 545

Javot H, Lauvergeat V, Santoni V, Martin-Laurent F, Güçlü J, Vinh J, Heyes J, Franck KI, Schäffner AR, Bouchez D, et al (2003) Role of a single aquaporin isoform in root water uptake. Plant Cell **15:** 509–522

Karimi M, Inzé D, Van Lijsebettens M, Hilson P (2013) Gateway vectors for transformation of cereals. Trends Plant Sci **18:** 1–4

Kubo M, Udagawa M, Nishikubo N, Horiguchi G, Yamaguchi M, Ito J, Mimura T, Fukuda H, Demura T (2005) Transcription switches for protoxylem and metaxylem vessel formation. Genes Dev **19:** 1855–1860

Lee SH, Chung GC, Jang JY, Ahn SJ, Zwiazek JJ (2012) Overexpression of PIP2;5 aquaporin alleviates effects of low root temperature on cell hydraulic conductivity and growth in Arabidopsis. Plant Physiol **159:** 479–488

Ma F, Peterson CA (2001) Frequencies of plasmodesmata in *Allium cepa* L. roots: Implications for solute transport pathways. J Exp Bot **52:** 1051–1061

Maurel C, Boursiac Y, Luu D-T, Santoni V, Shahzad Z, Verdoucq L (2015) Aquaporins in plants. Physiol Rev **95:** 1321–1358

Maurel C, Verdoucq L, Rodrigues O (2016) Aquaporins and plant transpiration. Plant Cell Environ **39:** 2580–2587

McCarty DR, Settles AM, Suzuki M, Tan BC, Latshaw S, Porch T, Robin K, Baier J, Avigne W, Lai J, et al (2005) Steady-state transposon mutagenesis in inbred maize. Plant J **44:** 52–61

McCarty DR, Suzuki M, Hunter C, Collins J, Avigne WT, Koch KE (2013) Genetic and molecular analyses of UniformMu transposon insertion lines. In T Peterson, ed, Plant Transposable Elements. Humana Press, Totowa, NJ, pp 157–166

Morsomme P, de Kerchove d'Exaerde A, De Meester S, Thinès D, Goffeau A, Boutry M (1996) Single point mutations in various domains of a plant plasma membrane H^+-ATPase expressed in *Saccharomyces cerevisiae* increase H^+-pumping and permit yeast growth at low pH. EMBO J **15:** 5513–5526

Moshelion M, Moran N, Chaumont F (2004) Dynamic changes in the osmotic water permeability of protoplast plasma membrane. Plant Physiol **135:** 2301–2317

Nelissen H, Rymen B, Jikumaru Y, Demuynck K, Van Lijsebettens M, Kamiya Y, Inzé D, Beemster GT (2012) A local maximum in gibberellin levels regulates maize leaf growth by spatial control of cell division. Curr Biol **22:** 1183–1187

Nelissen H, Sun XH, Rymen B, Jikumaru Y, Kojima M, Takebayashi Y, Abbeloos R, Demuynck K, Storme V, Vuylsteke M, et al (2018) The reduction in maize leaf growth under mild drought affects the transition between cell division and cell expansion and cannot be restored by elevated gibberellic acid levels. Plant Biotechnol J **16:** 615–627

Nour-Eldin HH, Hansen BG, Nørholm MH, Jensen JK, Halkier BA (2006) Advancing uracil-excision based cloning towards an ideal technique for cloning PCR fragments. Nucleic Acids Res **34:** e122

Parent B, Hachez C, Redondo E, Simonneau T, Chaumont F, Tardieu F (2009) Drought and abscisic acid effects on aquaporin content translate into changes in hydraulic conductivity and leaf growth rate: A trans-scale approach. Plant Physiol **149:** 2000–2012

Parent B, Turc O, Gibon Y, Stitt M, Tardieu F (2010) Modelling temperature-compensated physiological rates, based on the co-ordination of responses to temperature of developmental processes. J Exp Bot **61:** 2057–2069

Péret B, Li G, Zhao J, Band LR, Voß U, Postaire O, Luu D-T, Da Ines O, Casimiro I, Lucas M, Wells DM, Lazzerini L, et al (2012) Auxin regulates aquaporin function to facilitate lateral root emergence. Nat Cell Biol **14:** 991–998

Postaire O, Tournaire-Roux C, Grondin A, Boursiac Y, Morillon R, Schäffner AR, Maurel C (2010) A PIP1 aquaporin contributes to hydrostatic pressure-induced water transport in both the root and rosette of Arabidopsis. Plant Physiol **152:** 1418–1430

Prado K, Maurel C (2013) Regulation of leaf hydraulics: From molecular to whole plant levels. Front Plant Sci **4:** 255

Rodrigues O, Reshetnyak G, Grondin A, Saijo Y, Leonhardt N, Maurel C, Verdoucq L (2017) Aquaporins facilitate hydrogen peroxide entry into guard cells to mediate ABA- and pathogen-triggered stomatal closure. Proc Natl Acad Sci USA **114:** 9200–9205

Sack L, Holbrook NM (2006) Leaf hydraulics. Annu Rev Plant Biol **57:** 361–381

Sade N, Gebretsadik M, Seligmann R, Schwartz A, Wallach R, Moshelion M (2010) The role of tobacco Aquaporin1 in improving water use efficiency, hydraulic conductivity, and yield production under salt stress. Plant Physiol **152:** 245–254

Sade N, Shatil-Cohen A, Attia Z, Maurel C, Boursiac Y, Kelly G, Granot D, Yaaran A, Lerner S, Moshelion M (2014) The role of plasma membrane aquaporins in regulating the bundle sheath-mesophyll continuum and leaf hydraulics. Plant Physiol **166:** 1609–1620

Sadok W, Naudin P, Boussuge B, Muller B, Welcker C, Tardieu F (2007) Leaf growth rate per unit thermal time follows QTL-dependent daily patterns in hundreds of maize lines under naturally fluctuating conditions. Plant Cell Environ **30:** 135–146

Shatil-Cohen A, Attia Z, Moshelion M (2011) Bundle-sheath cell regulation of xylem-mesophyll water transport via aquaporins under drought stress: A target of xylem-borne ABA? Plant J **67:** 72–80

Shatil-Cohen A, Sibony H, Draye X, Chaumont F, Moran N, Moshelion M (2014) Measuring the osmotic water permeability coefficient (P_f) of spherical cells: Isolated plant protoplasts as an example. J Vis Exp (92): e51652

Siefritz F, Tyree MT, Lovisolo C, Schubert A, Kaldenhoff R (2002) PIP1 plasma membrane aquaporins in tobacco: From cellular effects to function in plants. Plant Cell **14:** 869–876

Steudle E (2000) Water uptake by plant roots: An integration of views. Plant Soil **226:** 45–56

Steudle E, Peterson CA (1998) How does water get through roots? J Exp Bot **49:** 775–788

Tyree MT, Nardini A, Salleo S, Sack L, El Omari B (2005) The dependence of leaf hydraulic conductance on irradiance during HPFM measurements: Any role for stomatal response? J Exp Bot **56:** 737–744

Vandeleur R K, Sullivan W, Athman A, Jordans C, Gilliham M, Kaiser B N, Tyerman S D (2014) Rapid shoot-to-root signalling regulates root hydraulic conductance via aquaporins. Plant Cell Environ **37:** 520–538

Volkov V, Fricke W, Hachez C, Moshelion M, Draye X, Chaumont F (2006) Osmotic water permeability differs between growing and non-growing barley leaf tissues. J Exp Bot **58:** 377–390

Wang C, Hu H, Qin X, Zeise B, Xu D, Rappel W-J, Boron WF, Schroeder JI (2016) Reconstitution of CO_2 regulation of SLAC1 anion channel and function of CO_2-permeable PIP2;1 aquaporin as CARBONIC ANHYDRASE4 interactor. Plant Cell **28:** 568–582

Zwieniecki MA, Thompson MV, Holbrook NM (2002) Understanding the hydraulics of porous pipes: Tradeoffs between water uptake and root length utilization. J Plant Growth Regul **21:** 315–323

Downloaded from https://academic.oup.com/plphys/article/182/4/2154/6116623 by universite catholique de louvain user on 08 October 2021